Official Journal of CIOMP
elight.springeropen.com

LETTER

Open Access

Two-photon MINFLUX with doubled localization precision

Kun Zhao[1,2], Xinzhu Xu[1,2], Wei Ren[1], Dayong Jin[3] and Peng Xi[1,3,4*]

Abstract

Achieving localization with molecular precision has been of great interest for extending fluorescence microscopy to nanoscopy. MINFLUX pioneers this transition through point spread function (PSF) engineering, yet its performance is primarily limited by the signal-to-background ratio. Here we demonstrate theoretically that two-photon MINFLUX (2p-MINFLUX) could double its localization precision through PSF engineering by nonlinear effect. Cramér-Rao Bound (CRB) is studied as the maximum localization precision, and CRB of two-photon MINFLUX is halved compared to single-photon MINFLUX (1p-MINFLUX) in all three dimensions. Meanwhile, in order to achieve same localization precision with 1p-MINFLUX, 2p-MINFLUX requires only 1/4 of fluorescence photons. Exploiting simultaneous two-photon excitation of multiple fluorophore species, 2p-MINFLUX may have the potential for registration-free nanoscopy and multicolor tracking.

Keywords: Super-resolution microscopy, Single-molecule localization, MINFLUX, Two-photon microscopy

1 Introduction

Super-resolution microscopy takes our vision from the conventional 200 nm diffraction limit down to 20 nm regime [1–8]. MINFLUX further extends the resolution to sub-10 nm [9–13], through combining STED-like coordinate-targeted excitation donut [1] and the coordinate-stochastic single-molecule localization microscopy (SMLM) [2, 3]. By engineering the point spread functions of the microscope, many techniques were introduced to break the precision confinement of localization [4–6, 14–16]. In MINFLUX [9–13], the excitation PSF is engineered to first-order Laguerre-Gaussian beam. Using the intensity minimum of coordinate-targeted confocal excitation, MINFLUX reduces much of the required photons, as intensity minimum has much higher contrast of intensity than intensity maximum of Gaussian excitation, thus is less prone to Poissonian noise [9, 17]. Yet, the full potential of MINFLUX has not been reached regarding acquisition time and signal-to-background ratio. Multiphoton microscopy features with a nonlinear dependence of the incidence to the excited signal, hence bear potential to further increase the spatio-temporal resolution of MINFLUX. For example, in two-photon microscopy, the fluorescence intensity is proportional to the square of excitation intensity [18–21]. The contrast at intensity minima of MINFLUX donut could be enhanced by the square dependence. Intuitively, together with that two-photon excitation decrease the out-of-focus fluorescence background, employing two-photon excitation to MINFLUX could significantly improve its localization precision. Here we give a theoretical framework of two-photon MINFLUX (2p-MINFLUX). We show explicitly that the square of fluorescence intensity results in 2-fold increase in maximum localization precision compared to 1p-MINFLUX. This suggests that only 1/4 photons are needed for achieving the same localization precision. Taking advantage of spectral overlapping of absorption for different fluorophore [22–24], 2p-MINFLUX may have the potential for registration-free multicolor localizations through emission spectral separation, which

*Correspondence: xipeng@pku.edu.cn
[1] Department of Biomedical Engineering, College of Future Technology, Peking University, Beijing 100871, China
Full list of author information is available at the end of the article

paves new avenue for simultaneous single particle tracking of fluorophores of different spectra.

2 Results

2.1 Localization precision

For a quantitative illustration, suppose an ideal zero-center donut excitation and a background-free condition with only Poissonian noise. Representing localization estimations with confidence intervals (Fig. 1a), the width of confidence interval for two-photon fluorescence localization is 1/2 of width for single-photon fluorescence, demonstrating improved localization precision.

To explicitly evaluate the improvement, Cramér-Rao Bound (CRB) is calculated for maximum localization precision of 2p-MINFLUX [9]. Modification is made on the Poissonian mean λ for two-photon fluorescence considering nonlinear effect:

$$\lambda_{1p}(\vec{r}_f) = f_1 I_{1p}(\vec{r}_f) \tag{1a}$$

$$\lambda_{2p}(\vec{r}_f) = f_2 I_{2p}^2(\vec{r}_f) \tag{1b}$$

where $\vec{r}_f$ is the fluorophore position, f_1 and f_2 stand for, for simplicity, factors corresponding to absorption cross-section of fluorophore, quantum yield and collection efficiency of the system, and I_{1p} and I_{2p} are point spread functions (PSF) of donut excitations. All other parameters in the model are kept unchanged.

CRB is expressed in an intricate general form of $\frac{\partial\lambda}{\partial x}$ and $\frac{\partial\lambda}{\partial y}$. As we show in Code File 1 (Ref. [25]), for the typical four-point targeted coordinate pattern (TCP) [9–13], at the origin where localization precision is highest (*i.e.*, minimum CRB), CRB can be expressed explicitly as [9]:

$$CRB_{1p}(\vec{0}) = \frac{L}{2\sqrt{2N}} \frac{s}{1 - \frac{L^2 \ln 2}{fwhm_{1p}^2}} \tag{2a}$$

$$CRB_{2p}(\vec{0}) = \frac{L}{4\sqrt{2N}} \frac{s}{1 - \frac{L^2 \ln 2}{fwhm_{2p}^2}} \tag{2b}$$

where L is the diameter of TCP circle, N is number of detected photons, *fwhm* is the full width at half maximum of the excitation PSF, and factor $s = \sqrt{\left(\frac{1}{SBR} + 1\right)\left(\frac{3}{4SBR} + 1\right)}$, where *SBR(L)* is the (median) signal-to-background ratio (dependent on L) [9, 12]. Since $L \ll fwhm_{1p} \leq fwhm_{2p}$, we can obtain precision increase slightly larger than two-fold:

$$CRB_{2p}(\vec{0}) \leq \frac{1}{2} CRB_{1p}(\vec{0}) \tag{3}$$

The reason for halving of CRB lies in that a factor of 2 appears when the square of I_{2p} is differentiated:

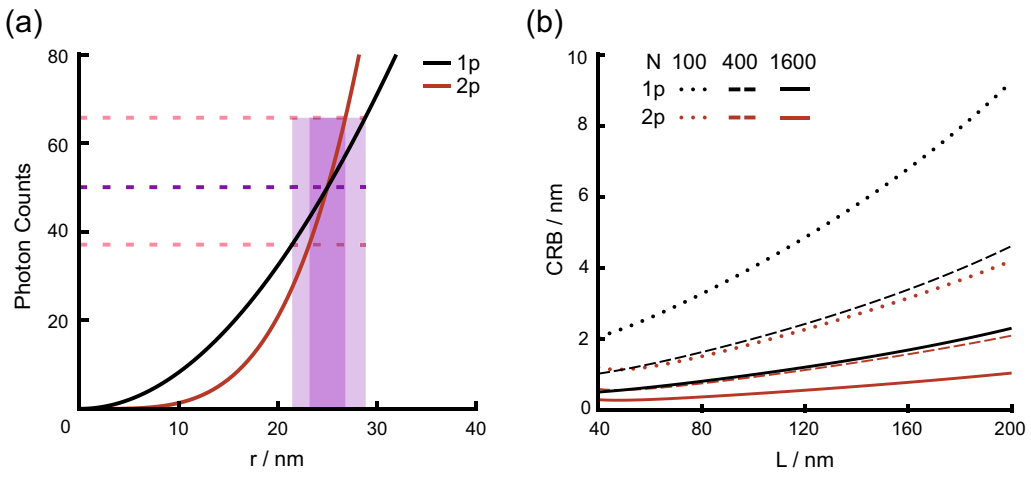

Fig. 1 Localization precision of 2p-MINFLUX. **a** Intuitive understanding of precision enhancement of 2p-MINFLUX. Length of 95 confidence interval of localized position is halved for two-photon fluorescence. Two curves shows single-photon and two-photon fluorescence intensities respectively . Assume Poissonian means for single-photon and two-photon fluorescence at $r = 25$ nm are both 50 (i.e., normalization at $r = 25$ nm), and assume detected photon is 50 as well. *fwhm* is calculated with NA=1.4, and single-photon and two-photon excitation wavelengths are set to 647 nm and 800 nm respectively. **b** Comparison of CRB between single-photon and two-photon MINFLUX with respect to N and L. CRB is calculated with given $SBR = 3$

$$\frac{\partial \lambda_{1p}}{\partial x} = \frac{\partial \left(f_1 I_{1p}\right)}{\partial x} = f_1 \frac{\partial I_{1p}}{\partial x} \tag{4a}$$

$$\frac{\partial \lambda_{2p}}{\partial x} = \frac{\partial \left(f_2 I_{2p}^2\right)}{\partial x} = 2 f_2 I_{2p} \frac{\partial I_{2p}}{\partial x} \tag{4b}$$

and that in CRB formula (see Eq.(S26) in [9]), the denominator has one more power of the above partial derivatives than the nominator, resulting in an additional factor of 2 in the denominator.

Maximum localization precision is compared for single-photon and two-photon MINFLUX with respect to N (Fig. 1b). For $L = 50$ nm, $SBR = 3$, $N = 100$, and single-photon and two-photon excitation wavelengths set to 647 nm and 800 nm, CRB_{2p} and CRB_{1p} are 1.15 nm and 2.31 nm respectively, with CRB enhancement ratio $R_{CRB} = CRB_{1p}/CRB_{2p} = 2.01$. In addition, 2p-MINFLUX possesses same or slightly higher localization precision with only 1/4 photons compared to 1p-MINFLUX ($N_{2p} = 100$ versus $N_{1p} = 400$, or $N_{2p} = 400$ versus $N_{1p} = 1600$).

Dependence on CRB of possible changes of parameters are considered (Fig. 2). Quite contrary to intuition, CRB decreases (*i.e.* localization precision increases) as excitation wavelength increases (Fig. 2a), which is different from traditional localization methods, where precision is proportional to excitation wavelength. CRB changes only slightly with different excitation wavelength, providing same *SBR* and *L*. We set single-photon excitation wavelength as 647 nm since red/crimson dyes were most commonly used in previous works [9–13], and two-photon excitation wavelength as 800 nm corresponding to these dyes [23, 24]. Longer wavelength with less phototoxicity such as 1280 nm [26] may also be considered; note that with 1280 nm excitation, *SBR* may be compromised due to increased background from an enlarged PSF and decreased signal from extended intensity minima.

With $L_0 = 50$ nm fixed, improved *SBR* results in increased localization precision (i.e., decreased CRB)

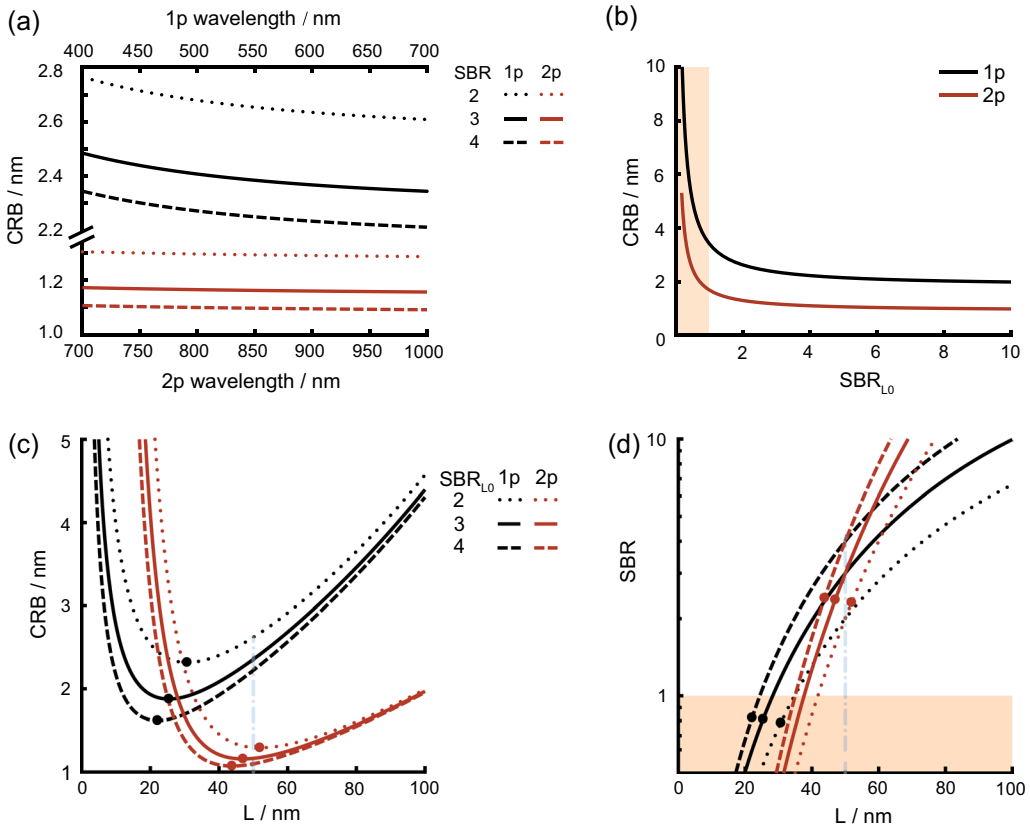

Fig. 2 Dependence of CRB on different parameters. **a** Dependence of CRB with respect to *SBR* and excitation wavelength. CRB is calculated with given $L = 50$ nm and $N = 100$. **b** Dependence of CRB with respect to *SBR* with fixed *L*. In the shaded area where (median) $SBR \lesssim 1$, CRB increases (precision decreases) sharply. **c**, **d** Combined influence on CRB by *SBR* and *L*. *SBR* is given at $L_0 = 50$ nm (blue lines). *SBR* decreases as *L* decreases (**d**), sets a lower bound for *L* (**c**). At optimal CRB (solid dots), $SBR_{1p} \approx 0.81$, $SBR_{2p} \approx 2.36$. Note the logarithmic scale for SBR (**d**). CRB is calculated with $N = 100$ for (**b**–**d**)

(Fig. 2b). If *SBR* decreases to ≤ 1, then precision decreases sharply, due to the inverse proportion of *SBR* to CRB as in factor *s*. Thus circumstances with $SBR \leq 1$ should be avoided as much as possible ($SBR \leq 1$ is not a good parameter for any imaging technique).

We then consider the combined influence on CRB of *SBR* and *L* (Fig. 2c, d). *SBR* decreases as *L* decreases (Fig. 2d). Given a fixed *SBR* at $L_0 = 50$ nm, there is a lower bound of CRB and a corresponding optimal *L* (denoted as L_{opt}) (Fig. 2c). We argue that given the limited *SBR* as MINFLUX uses donut minimum, decrease of *L* below 50 nm and to L_{opt} is not fruitful as it first seems. Note that *SBR* is not constant; median *SBR* is used to its distribution and ranges around 1.4 to 4.2 for biological samples at $L = 50$ nm [12]. For 1p-MINFLUX, median $SBR \approx 0.81$ (Fig. 2d) at L_{opt}, which suggests that *SBR* is $\leq$ 0.81 in 50 percent localizations and thus attainable CRB is impaired. For 2p-MINFLUX, *SBR* decreases more rapidly with *L* compared to 1p-MINFLUX (Fig. 2d), limiting further decrease of *L* (Fig. 2c). To make direct comparison, same $L = 50$ nm and median $SBR = 3$ are used for both 1p-MINFLUX and 2p-MINFLUX.

CRB across 2D xy-plane for one-photon and two-photon MINFLUX is compared for $L = 50$ nm (Fig. 3). Of most interest is only CRB in center region of TCP circle instead of whole xy-plane, since a previous round of iterative 1p-MINFLUX with $L = 100$ nm already localizes the fluorophore with single-digit nanometer precision (*e.g.* 3.3 nm) [12]. A center region with radius of 3.3 nm has consistently $R_{CRB} \geq 1.92$. (Note that in iterative 2p-MINFLUX, a second-last round with $L = 100$ nm would likely obtain precision better than 3.3 nm as well, resulting in further improved R_{CRB}.) CRB increases (precision decreases) with increasing *r*; 2p-MINFLUX has faster increase of CRB than 1p-MINFLUX (Additional file 1: Figure S1a, b), resulting in decrease of R_{CRB} with increasing *r* (Fig. 3c, d). This faster increase could be explained by the faster decrease of intensity of 'signal'

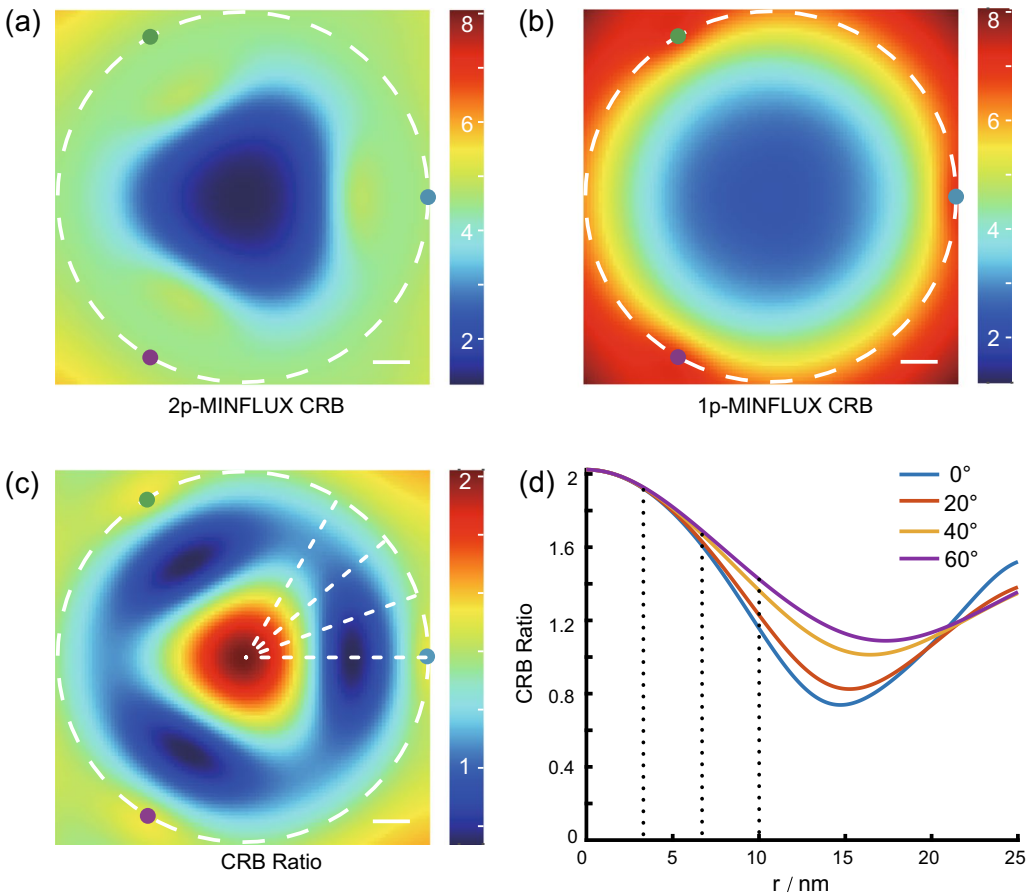

Fig. 3 Comparison of CRB of 2p-MINFLUX versus 1p-MINFLUX in xy-plane. **a**, **b** Comparison of CRB across xy-plane of (**a**) 2p-MINFLUX and (b) 1p-MINFLUX. Colormaps are rescaled into same dynamic range. CRB is calculated with $N = 100$, $L = 50$ nm, and $SBR = 3$. **c** Ratio of CRB of 1p-MINFLUX to 2p-MINFLUX in (**a**, **b**). Dotted lines represent directions for 1D profiles in (**d**). **d** 1D cut profiles of CRB ratio in (**c**). 4 angles (0, 20, 40, 60) are chosen considering symmetry. Three dotted lines represent $r = 1\sigma$, 2σ and 3σ. Scale bar: **a**–**c** 5 nm

in 2p-MINFLUX compared to 1p-MINFLUX (Additional file 1: Supplementary note 1). At radius of 6.7 nm and 10.0 nm (representing 2σ and 3σ), average R_{CRB} are 1.67 and 1.31 respectively. In addition, 2p-MINFLUX CRB (Fig. 3a, S1a) is much more anisotropic than 1p-MINFLUX CRB (Fig. 3b, S1b); a triangle-like contour can be seen in CRB of 2p-MINFLUX (Fig. 3a), but not in 1p-MINFLUX CRB (Fig. 3b). This could also be explained qualitatively by plotting the different 'signals': in 2p-MINFLUX, 'signals' decreases faster with r for angle 0 than angle 60 (Additional file 1: Supplementary note 1). Anisotropy also exists for CRB under $L = 100$ nm (Additional file 1: Supplementary note 2, Figure S2).

The enhancement of z-localization precision is similar to xy-localization. 3D-donut is modeled simply as a quadratic function [12]. The highest precision at the origin also increases by 2-fold:

$$CRBz_{1p}(\vec{0}) = \frac{L}{4\sqrt{N}}\left(\frac{1}{SBR}+1\right) \tag{5a}$$

$$CRBz_{2p}(\vec{0}) = \frac{L}{8\sqrt{N}}\left(\frac{1}{SBR}+1\right) \tag{5b}$$

2.2 Localization reconstruction

Using maximum likelihood estimation (MLE), z-axis localization, as a 1D problem, can be solved analytically for 2p-MINFLUX as well:

$$\hat{z}_{2p}^{(MLE)} = -\frac{L}{2} + \frac{L}{1+\sqrt[4]{\frac{n_1}{n_0}}} \tag{6}$$

where n_0 and n_1 are number of photons detected with $I\left(-\frac{L}{2}\right)$ and $I\left(\frac{L}{2}\right)$. Imaginary roots and a real root outside of $\left(-\frac{L}{2}, \frac{L}{2}\right)$ are neglected. In simulation, the above estimator agrees with ground truth, and improved localization precision can be seen (Fig. 4).

For localization estimation in xy-plane, we investigated two methods: maximum likelihood estimation (MLE) and least mean square estimation (LMS), being unbiased and biased respectively. For LMS estimation, a same first-order linearization is used [9]. The LMS estimator can be analytically solved:

$$\hat{\vec{r}}_{1p}^{(LMS)} = -\frac{1}{1-\frac{L^2\ln 2}{fwhm_{1p}^2}}\sum_{i=1}^{k}\hat{p}_i\vec{r}_i \tag{7a}$$

$$\hat{\vec{r}}_{2p}^{(LMS)} = -\frac{1}{2}\frac{1}{1-\frac{L^2\ln 2}{fwhm_{2p}^2}}\sum_{i=1}^{k}\hat{p}_i\vec{r}_i \tag{7b}$$

where k is the number of exposures, and, $\hat{p}_i = n_i/N$, where n_i and $\vec{r}_i$ are, respectively, number of collected photons and displacement of excitation beam for each exposure. Similar to the expression of CRB, denominator of LMS estimator is also multiplied by a factor of 2.

For MLE estimation, the log-likelihood function is maximized as classically done. The maximization is solved numerically. MLE estimation should be given a starting value for its convergence. In our simulation, LMS estimator served as this starting value thanks to its simple form. We simulated MINFLUX imaging in xy-plane for $L = 50$ nm with numerically solved MLE estimation (Fig. 5). For photon number $N = 250$, 2p-MINFLUX can already achieve 6 nm resolution, which is barely feasible in 1p-MINFLUX (Fig. 5b, c). In addition, compared with 1p-MINFLUX with $N = 1000$ (Fig. 5d), 2p-MINFLUX with $N = 250$ achieved similar localization distributions, confirming the capability of 2p-MINFLUX to reduce number of photons required.

We believe 2p-MINFLUX would be capable of multicolor localizations (Fig. 5e, f). Because of the spectral overlapping of two-photon absorption peaks, it is possible to excite multiple fluorophores simultaneously. If emission spectra of the multiple fluorophores

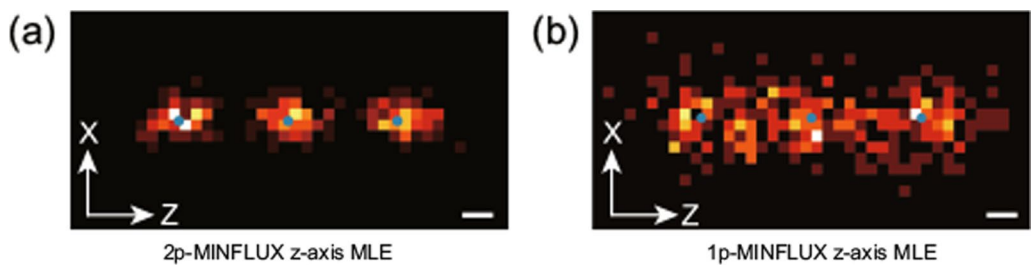

Fig. 4 Simulation of z-axis localization. A structure with 3 positions was simulated, with z-coordinates being -5, 0, 5 nm for each positions. To focus solely on z-localizations, *x*-positions are not reconstructed with MINFLUX and are generated with normal random number for visualization; parameters are set as: standard deviation $\sigma_{1p} = 1.0$ nm, $\sigma_{2p} = 0.5$ nm, and mean $\mu_{1p} = \mu_{2p} = 0$. Calculation is conducted with $N = 100$, $L = 50$ nm, and $SBR = 3$. Pixel size is 0.5 nm. Scale bar: 1 nm

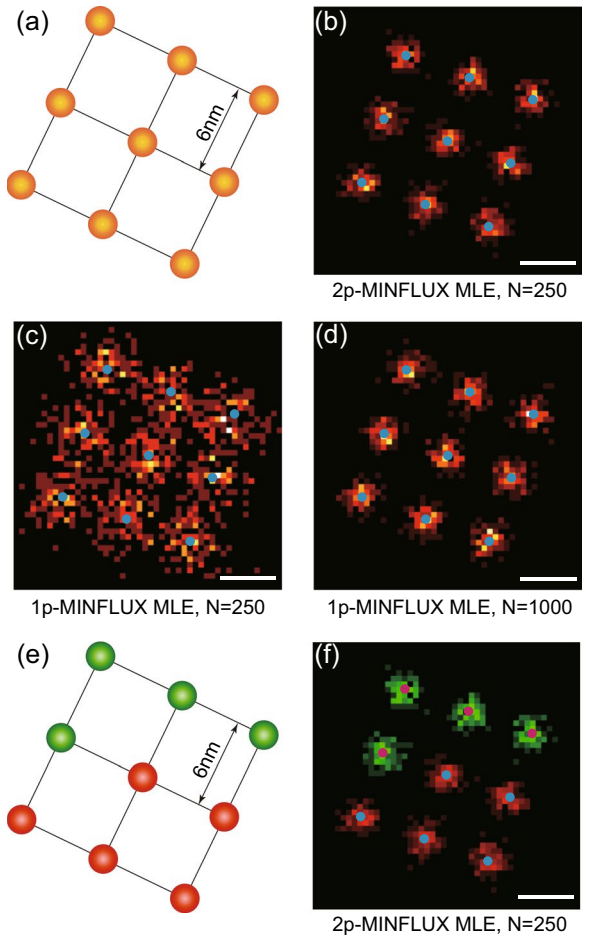

Fig. 5 Simulation results of 2p-MINFLUX. **a** Configuration of a simulated single-color dye-labelled square DNA origami. (b-d) Simulation on the above origami of **b** 2p-MINFLUX and **c**, **d** 1p-MINFLUX. For each dye, simulation of localization was repeated for **b**, **d** 25 and **c** 100 times respectively, with $N = 250$ (**b**, **c**) or 1000 (**d**), $L = 50$ nm, and $SBR = 3$. Pixel size is 0.5 nm. **e** Configuration of a simulated dual-color dye-labelled origami for simulation of dual-color 2p-MINFLUX. Angles and distances are same with (**a**). **f** Simulation of dual-color 2p-MINFLUX. Simulation was repeated for 100 times for each dye, with $N = 250$, $L = 50$ nm, and $SBR = 3$. Scale bar: **b**–**d**, and **f** 5 nm

are not overlapped, then complete separation of different fluorescence can be achieved with simple dichromatic filters. Although it is not a must to use a single excitation for multicolor two-photon microscopy, a single-wavelength two-photon excitation is beneficial for multicolor MINFLUX, as it can be easily achieved with dichromatic beam splitters. In this configuration, multicolor 2p-MINFLUX would be free of registration of different color channels, as they are excited with the same donut coordinates. Hence, this may enable simultaneous registration-free multicolor MINFLUX tracking, which could be crucial for study of molecular interactions. Note that L could be adjusted dynamically, and that since CRB worsens with increased r (Fig. 3), simultaneous localization gains most benefit only when fluorophores are close enough to the coordinate origin of excitation pattern.

3 Discussion

In future experimental works, attention needs to be paid on choice of fluorophores, choice of wavelength of femtosecond laser, power of two-photon excitation, attainable fluorescence rate, possible faster bleaching, and attainable signal-to-background ratio.

3.1 Overview

Increase of excitation power is needed in MINFLUX to achieve enough fluorescence rate compared to confocal laser scanning microscopy (CLSM) [10]; as L decreases, excitation power should be increased as well [12]. Figure 6 compares the intensities of excitation PSFs and emission PSFs of 2p-MINFLUX and 1p-MINFLUX with $L = 50$ nm.

Assume under certain excitation power P_a and P_b for 1p-donut and 2p-donut respectively [with peak intensity of excitation PSF being I_a and I_b respectively (Fig. 6a)], the fluorescence intensities are the same for fluorophores located exactly at the PSF peaks (with normalization of 1) (Fig. 6b). Intensities at $r = 25$ nm are low for both 2p-donut and 1p-donut (0.0543 and 0.0832 respectively) (Fig. 6a). In order to maximize fluorescence signals at $r = 25$ nm, excitation intensity (and power) of the excitation donut should be increased. Increase of $\approx$ 12.1-fold and 18.4-fold respectively for 1p-/2p-MINFLUX (Fig. 6c) would result in same fluorescence signals (with value of 1) at $r = 25$ nm for MINFLUX (Fig. 6d) compared with the original donut (Fig. 6a, b). For 2p-MINFLUX, the fold of increase remains comparable with 1p-MINFLUX; an additional 1.5-fold only is sufficient.

Hypothetical emission donuts for 1p-/2p-MINFLUX could be derived as well (Fig. 6d). The intensity of peak for 1p-MINFLUX emission donut is 12.1, whereas for 1p-MINFLUX emission donut is $18.4^2 = 338$ because of the square dependence. We argue that curves in Fig. 6(d) do not reflect reality because of fluorescence saturation (Additional file 1: Supplementary note 3) and fluorophores being in single-molecule state (see subsection 4 'Background' of Discussion).

3.2 Estimated fluorescence rate

The useful fluorescence rate (denoted as η_{MFX}) in 1p-MINFLUX is $\eta_{1pMFX} \leq 50$ kHz for the dyes AF647, CF680 and CF660C [12].

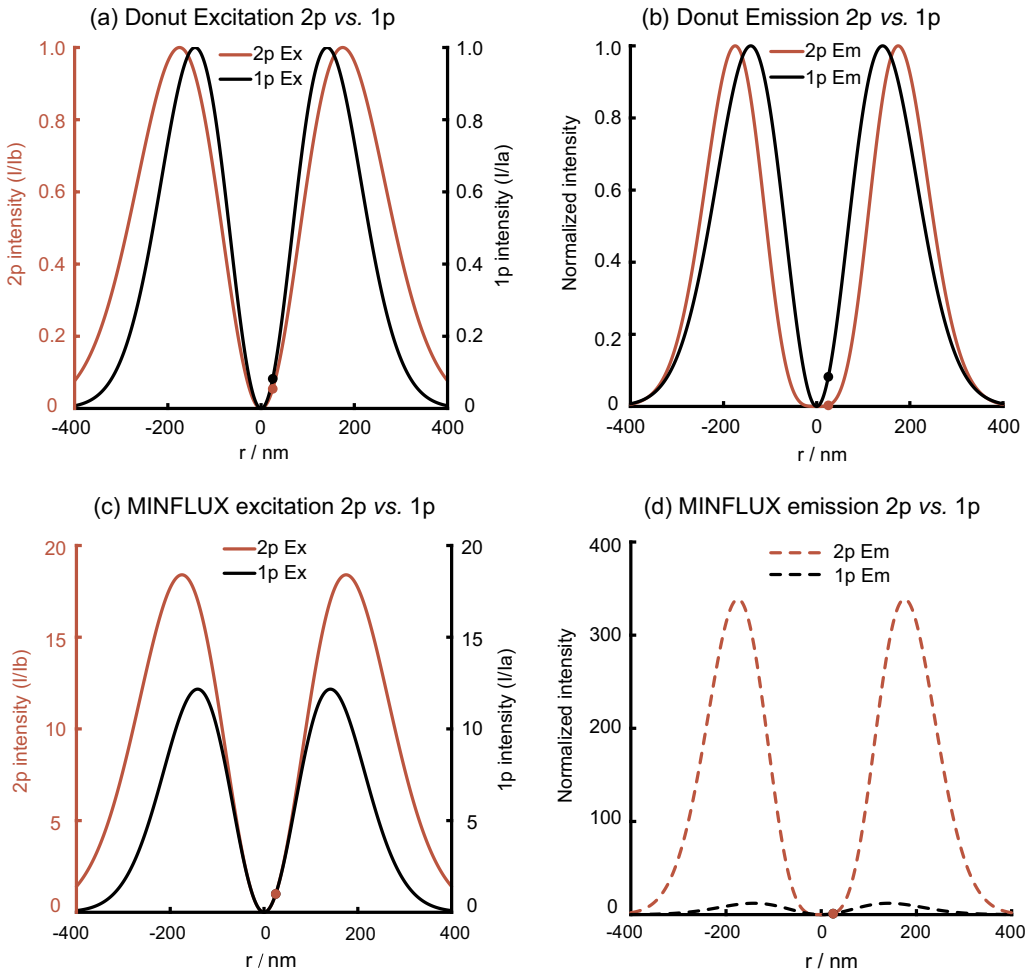

Fig. 6 Profiles of excitation and emission intensities of 2p-MINFLUX and 1p-MINFLUX. Solid dots indicate donut intensities at $r = 25$ nm. Donut peaks occur at radius $r_{1p} = 142$ nm, and $r_{2p} = 175$ nm, corresponding to a 1.24-fold increase. **a**, **b** Donut excitation and emission similar to traditional confocal. Excitation intensities at $r = 25$ nm are $I_{1p} = 0.0832 \approx 1/12.1$, and $I_{2p} = 0.0543 \approx 1/18.4$. **c**–**d** MINFLUX donut profiles with increased excitation power. Excitation power is increased by 12.1-fold and 18.4-fold for 1p-/2p-MINFLUX respectively (**c**). Intensities in **d** is only hypothetical; considering fluorescence saturation, curves of emission would reach plateau (saturation) beyond certain values of r

Before discussion on fluorescence rate and possible saturation in MINFLUX, basic characteristics of the relationship between fluorescence rate and excitation power for both one-photon and two-photon fluorescence should be explicated. The relationship is often shown with curves of fluorescence rate to excitation power. Each curve of fluorescence rate can be separated into two parts: a first part with strict linear (for one-photon) or quadratic (for two-photon) power dependence, and a second part that reaches plateau [27–30]. We use denotations η_{lin} (η_{1lin} or η_{2lin}) to describe the maximum fluorescence rate with linear (or quadratic, respectively) power dependence for single-photon or two-photon fluorescence (i.e., at the transition point from linear to nonlinear (saturation) dependence); and η_{sat} (η_{1sat} or η_{2sat}) to describe the saturated fluorescence rate. A non-saturated, strictly displacement-dependent fluorescence should be ensured for either 1p-/2p-MINFLUX. Regions of interest (ROIs) should be quantified; for $L = 50$ nm ($r_0 = 25$ nm), the radius r of the fluorophore can be described as $r_0 \pm 3\sigma$, where σ is the CRB of a previous round of iteration with $L = 100$ nm. For a strictly linear/quadratic dependence within the ROIs, $\eta_{r_0 \pm 3\sigma} \leq \eta_{lin}$ should be satisfied ($\eta_{r_0 \pm 3\sigma} = \eta_{lin}$ to maximize the fluorescence detection of MINFLUX). Thus MINFLUX fluorescence rate is estimated as

$$\eta_{MFX} = \eta_{r_0} = \frac{I(r_0)}{I(r_0 + k\sigma)} \eta_{r+k\sigma} \leq \frac{I(r_0)}{I(r_0 + k\sigma)} \eta_{lin} \tag{8}$$

For 1p-MINFLUX with $\sigma_{1p} = 3.3$ nm, $\frac{I(r_0+k\sigma)}{I(r_0)} = 1.90$; while for 2p-MINFLUX with $\sigma_{2p} = 1.6$ nm (Additional file 1: Supplementary note 4), and $\frac{I(r_0+k\sigma)}{I(r_0)} = 2.04$.

Data of η_{2lin} for the red/crimson dyes were not found in literature. We assume that the ratios of $\frac{\eta_{2lin}}{\eta_{1lin}}$ are the same for different fluorophores. For the dye TMR [27], $\eta_{1lin} = 20$ kHz, and $\eta_{2lin} = 13$ kHz. Thus the fluorescence rate for 2p-MINFLUX could be estimated as $\eta_{2pMFX} \approx \frac{\eta_{2lin}}{\eta_{1lin}} \frac{1.90}{2.04} \eta_{1pMFX} = 30$ kHz. A smaller rate of 25 kHz is chosen, corresponding to collected photons $N = 1000$ in $t = 40$ ms exposure time. Indeed, the fluorescence rate would be smaller for two-photon fluorescence than single-photon fluorescence. The realistic fluorescence rate achievable should be measured in experiment.

Although the out-of-focus noise is almost absent for two-photon excitation, pulsed two-photon excitation may cause faster bleaching than continuous-wave single-photon excitation at the focal plane. This may limit the attainable number of repeats of localizations per molecule of 2p-MINFLUX.

3.3 Estimated excitation power

The excitation power needed for 2p-MINFLUX is calculated (Additional file 1: Supplementary Note 5). Equation (9) in ref. [20] is used for calculation. Two-photon cross-sections of 100 GM is mainly considered; several red/crimson dyes (Atto647N, Silicon Rhodamine, STAR 635P, Atto594 and Atto590) all have > 100GM cross sections under 800 nm excitation [24]. For a fluorophore with 100 GM two-photon cross section, < 1 mW of confocal excitation power is enough for fluorescence rate to reach 25 kHz for a single molecule (Additional file 1: Figure S3a). With a 18.4-fold decrease of intensities at $r = 25$ nm, excitation power of < 20 mW should be enough for 2p-MINFLUX (Additional file 1: Figure S3b). According to the ref. [26], with a 775 nm laser of 82 MHz repetition rate, 60 mW and 52 mW excitation power at sample surface were used for *ex vivo* and *in vivo* deep brain two-photon microscopy respectively. Of course, because of tissue scattering, the focal excitation power (not estimated in the reference) is not as large as 52 mW, the reference still shows that 52 mW power of femtosecond laser is compatible with biological settings.

3.4 Background

We maintain that the background of 2p-MINFLUX remain comparable to 1p-MINFLUX. Indeed, increase of excitation intensity would result in increase of background of 1p-MINFLUX compared to 1p-confocal, and also increase of background of 2p-MINFLUX compared to 2p-confocal. We argue that background in 1p-/2p-MINFLUX consists of two kinds of background: (1) background originated from outer region of focal donut PSF, and (2) out-of-focus background (originated from excitation outside focal PSF and arrived at detector due to scattering). Two-photon excitation would reduce the latter kind of background compared to 1p-MINFLUX, because of the restriction of two-photon excitation in the focal spot. However, 2p-MINFLUX may increase the first kind of background. Since the donut is larger for 2p-MINFLUX, there is increased possibility of two-photon-induced luminescence of unstained features (excited with elevated excitation intensities although they have limited two-photon cross-sections).

Importantly, both 1p-MINFLUX and 2p-MINFLUX are single-molecule localization microscopy (SMLM) technique, not simple confocal laser scanning microscopy. There would not be excessive fluorescence background (no 12-fold or 338-fold for 1p-/2p-MINFLUX) originated from another molecule because (1) other molecules are in off-state; and (2) if an off-state molecule is turned on unwantedly, the molecule would be saturated because fluorescence saturation would occur at $r >> 25$ nm, and this particular data should be discarded. However, because of the larger radius compared to Gaussian PSFs in CLSM, 1p-MINFLUX necessitates higher requirement of single-molecule state; and 2p-MINFLUX may necessitate even higher requirement than 1p-MINFLUX because of its larger radius than 1p-donut as well.

4 Conclusion

In summary, MINFLUX can be enhanced with multiphoton excitation process, with 2-fold increase of localization precision or 4-fold decrease of required fluorescence photons compared to 1p-MINFLUX. As different dyes can be excited simultaneously with two-photon excitation, 2p-MINFLUX may have the potential for registration-free multicolor localizations. This may be of use not only for nanometer-precision localization microscopy [11, 12], but also simultaneous tracking [10] of several fluorophores. This could be crucial for study of molecular interactions, for example, protein-protein interactions, protein-nucleic acids interactions, or virus-cell interactions.

Abbreviations

CLSM: Confocal laser scanning microscopy; CRB: Cramér-Rao bound; *fwhm*: Full width at half maximum; 1p-MINFLUX: Single-photon MINFLUX; 2p-MINFLUX: Two-photon MINFLUX; MLE: Maximum-likelihood estimation; LMS: Least mean square estimation; NA: Numerical aperture; PSF: Point spread function; SBR: Signal-to-background ratio; SMLM: Single-molecule localization microscopy; STED: Stimulated emission depletion; TCP: Targeted coordinate pattern.

Supplementary Information

The online version contains supplementary material available at https://doi.org/10.1186/s43593-021-00011-x.

Additional file 1: Figure S1. CRB anisotropy for 2p-MINFLUX. **Figure S2**. Comparison of CRB with $L = 100$ nm. **Figure S3**. Power dependencies of single molecule emission rates for EGFP (a) and TMR (b). **Figure S4**. Progression of spatially averaged CRB of iteration 2p-MINFLUX and 1p-MINFLUX in 2D xy-plane. **Figure S5**. Excitation power needed for 2p-MINFLUX. **Table S1**. Single molecule emission rates for TMR and EGFP for single-photon and two-photon excitation of Figure S3. [2]. **Table S2**. Relationship of MINFLUX fluorescence rate $\eta_{minflux}$ to η_{lin} and η_{sat}. **Table S3**. CRBs in each round of iteration MINFLUX in xy-plane. **Table S4**. Parameters used in calculation of excitation power needed for 2p-MINFLUX.

Acknowledgements
Not applicable.

Authors' contributions
KZ and PX conceived the project. PX and DJ supervised the research. KZ, XX and WR performed the analysis and simulation, prepared the figures and wrote the manuscript. All authors participated in discussion and editing of the manuscript. All authors read and approved the final manuscript.

Funding
This work was supported by the Beijing Natural Science Foundation (JQ18019), the National Natural Science Foundation of China (62025501, 31971376, 61729501), the State Key Research Development Program of China (2017YFC0110202), and Shenzhen Science and Technology Program (KQTD20170810110913065).

Availability of data and materials
Data underlying the results presented in this paper are calculated or simulated with Code 1, Ref. [25].

Declarations

Ethics approval and consent to participate
Not applicable.

Consent for publication
Not applicable.

Competing interests
The authors declare that they have no competing interests.

Author details
[1]Department of Biomedical Engineering, College of Future Technology, Peking University, Beijing 100871, China. [2]Wallace H. Coulter Department of Biomedical Engineering, Georgia Institute of Technology and Emory University, Atlanta, 30332 Georgia, USA. [3]UTS-SUStech Joint Research Centre for Biomedical Materials & Devices, Department of Biomedical Engineering, College of Engineering, Southern University of Science and Technology, Shenzhen, Guangdong 518055, China. [4]National Biomedical Imaging Center, Peking University, Beijing 100871, China.

Received: 1 September 2021 Revised: 10 December 2021 Accepted: 22 December 2021
Published online: 25 March 2022

References

1. S.W. Hell, J. Wichmann, Breaking the diffraction resolution limit by stimulated emission: stimulated-emission-depletion fluorescence microscopy. Opt. Lett. **19**(11), 780–782 (1994)
2. E. Betzig, G.H. Patterson, R. Sougrat, O.W. Lindwasser, S. Olenych, J.S. Bonifacino, M.W. Davidson, J. Lippincott-Schwartz, H.F. Hess, Imaging intracellular fluorescent proteins at nanometer resolution. Science **313**(5793), 1642–1645 (2006)
3. M.J. Rust, M. Bates, X. Zhuang, Stochastic optical reconstruction microscopy (storm) provides sub-diffraction-limit image resolution. Nat. Methods **3**(10), 793 (2006)
4. S.R.P. Pavani, M.A. Thompson, J.S. Biteen, S.J. Lord, N. Liu, R.J. Twieg, R. Piestun, W. Moerner, Three-dimensional, single-molecule fluorescence imaging beyond the diffraction limit by using a double-helix point spread function. Proc. Natl. Acad. Sci. **106**(9), 2995–2999 (2009)
5. S. Jia, J.C. Vaughan, X. Zhuang, Isotropic three-dimensional super-resolution imaging with a self-bending point spread function. Nat. Photonics **8**(4), 302–306 (2014)
6. M.P. Backlund, Y. Shechtman, R.L. Walsworth, Fundamental precision bounds for three-dimensional optical localization microscopy with poisson statistics. Phys. Rev. Lett. **121**(2), 023904 (2018)
7. P. Fei, J. Nie, J. Lee, Y. Ding, S. Li, H. Zhang, M. Hagiwara, T. Yu, T. Segura, C.-M. Ho, D. Zhu, T.K. Hsiai, Subvoxel light-sheet microscopy for high-resolution high-throughput volumetric imaging of large biomedical specimens. Adv. Photonics **1**(1), 016002 (2019)
8. E. Narimanov, Resolution limit of label-free far-field microscopy. Adv. Photonics **1**(5), 056003 (2019)
9. F. Balzarotti, Y. Eilers, K.C. Gwosch, A.H. Gynnå, V. Westphal, F.D. Stefani, J. Elf, S.W. Hell, Nanometer resolution imaging and tracking of fluorescent molecules with minimal photon fluxes. Science **355**(6325), 606–612 (2017)
10. Y. Eilers, H. Ta, K.C. Gwosch, F. Balzarotti, S.W. Hell, Minflux monitors rapid molecular jumps with superior spatiotemporal resolution. Proc. Natl. Acad. Sci. **115**(24), 6117–6122 (2018)
11. J.K. Pape, T. Stephan, F. Balzarotti, R. Büchner, F. Lange, D. Riedel, S. Jakobs, S.W. Hell, Multicolor 3d minflux nanoscopy of mitochondrial micos proteins. Proc. Natl. Acad. Sci. **117**(34), 20607–20614 (2020)
12. K.C. Gwosch, J.K. Pape, F. Balzarotti, P. Hoess, J. Ellenberg, J. Ries, S.W. Hell, Minflux nanoscopy delivers 3d multicolor nanometer resolution in cells. Nat. Methods **17**(2), 217–224 (2020)
13. L.A. Masullo, F. Steiner, J. Zähringer, L.F. Lopez, J. Bohlen, L. Richter, F. Cole, P. Tinnefeld, F.D. Stefani, Pulsed interleaved minflux. Nano Lett. **21**(1), 840–846 (2021)
14. S.W. Hell, E.H. Stelzer, S. Lindek, C. Cremer, Confocal microscopy with an increased detection aperture: type-b 4pi confocal microscopy. Opt. Lett. **19**(3), 222–224 (1994)
15. M.G. Gustafsson, D. Agard, J. Sedat, I5m: 3d widefield light microscopy with better than 100nm axial resolution. J. Microsc. **195**(1), 10–16 (1999)
16. J. Bewersdorf, R. Schmidt, S.W. Hell, Comparison of i5m and 4pi-microscopy. J. Microsc. **222**(2), 105–117 (2006)
17. J. Xiao, T. Ha, Flipping nanoscopy on its head. Science **355**(6325), 582–584 (2017)
18. W.L. Peticolas, J.P. Goldsborough, K. Rieckhoff, Double photon excitation in organic crystals. Phys. Rev. Lett. **10**(2), 43 (1963)
19. C.J.R. Sheppard, M. Gu, Image formation in two-photon fluorescence microscopy. Optik (Stuttgart) **86**(3), 104–106 (1990)
20. W. Denk, J.H. Strickler, W.W. Webb, Two-photon laser scanning fluorescence microscopy. Science **248**(4951), 73–76 (1990)
21. W. Denk, D.W. Piston, W.W. Webb, Multi-photon molecular excitation in laser-scanning microscopy. In: Handbook of Biological Confocal Microscopy (Springer, Boston, MA 2006), pp. 535–549
22. F. Bestvater, E. Spiess, G. Stobrawa, M. Hacker, T. Feurer, T. Porwol, U. Berchner-Pfannschmidt, C. Wotzlaw, H. Acker, Two-photon fluorescence absorption and emission spectra of dyes relevant for cell imaging. J. Microsc. **208**(2), 108–115 (2002)
23. J. Mütze, V. Iyer, J.J. Macklin, J. Colonell, B. Karsh, Z. Petrášek, P. Schwille, L.L. Looger, L.D. Lavis, T.D. Harris, Excitation spectra and brightness optimization of two-photon excited probes. Biophys. J. **102**(4), 934–944 (2012)
24. M.G.M. Velasco, E.S. Allgeyer, P. Yuan, J. Grutzendler, J. Bewersdorf, Absolute two-photon excitation spectra of red and far-red fluorescent probes. Opt. Lett. **40**(21), 4915–4918 (2015)
25. K. Zhao, X. Xu, W. Ren, D. Jin, P. Xi, Code for 2p-MINFLUX simulation. github (2021), https://github.com/kunzhao1220/2pMINFLUX

26. D. Kobat, M.E. Durst, N. Nishimura, A.W. Wong, C.B. Schaffer, C. Xu, Deep tissue multiphoton microscopy using longer wavelength excitation. Opt. Express **17**(16), 13354–13364 (2009)
27. P. Schwille, U. Haupts, S. Maiti, W.W. Webb, Molecular dynamics in living cells observed by fluorescence correlation spectroscopy with one- and two-photon excitation. Biophys. J. **77**(4), 2251–2265 (1999)
28. K.G. Heinze, A. Koltermann, P. Schwille, Simultaneous two-photon excitation of distinct labels for dual-color fluorescence crosscorrelation analysis. Proc. Natl. Acad. Sci. **97**(19), 10377–10382 (2000)
29. P.S. Dittrich, P. Schwille, Photobleaching and stabilization of fluorophores used for single-molecule analysis with one- and two-photon excitation. Appl. Phys. B **73**(8), 829–837 (2001)
30. J. Mütze, Z. Petrášek, P. Schwille, Independence of maximum single molecule fluorescence count rate on the temporal and spectral laser pulse width in two-photon fcs. J. Fluoresc. **17**(6), 805–810 (2007)